JOURNAL OF THERMOPHYSICS AND HEAT TRANSFER
Vol. 24, No. 4, October–December 2010

Technical Notes

Optimization and Comparative Study on Oblique- and Rectangular-Fin Microchannel Heat Sinks

Danish Ansari, Afzal Husain, and Kwang-Yong Kim*
Inha University, Incheon 402-751, Republic of Korea

DOI: 10.2514/1.50162

Nomenclature

A_c	=	cross-sectional area of microchannels, m^2
A_s	=	surface area of the base substrate, m^2
H_c	=	depth of microchannels, 0.0004 m
L_f	=	length of fin, m
L_g	=	length of gap, m
L_x	=	length of the heat sink, 0.01 m
L_y	=	width of the heat sink, 0.01 m
L_z	=	height of the heat sink, 0.0005 m
$\dot{m}$	=	mass flow rate, kg/s
n	=	number of microchannels
P	=	pumping power, W
p_c	=	pitch of channel, m
p_x	=	pitch of fins in x direction, m
q	=	heat flux, 1.0e6 W/m^2
R_{th}	=	thermal resistance, K/W
T	=	temperature, K
u_{avg}	=	average coolant velocity in microchannels, m/s
W_b	=	thickness of substrate, 0.0001 m
W_c	=	width of microchannels, m
W_f	=	width of fins, m
x, y, z	=	orthogonal coordinate system
α	=	design variable p_c/H_c
β	=	design variable W_f/p_c
γ	=	design variable L_f/p_x
Δp	=	pressure drop, Pa
θ	=	oblique angle

Subscripts

f	=	fluid (liquid)
i	=	inlet
max	=	maximum value
o	=	outlet
s	=	substrate

I. Introduction

ADVANCEMENTS in microfabrication technology have helped considerably in increasing the performance of microchips by squeezing a large number of components in a smaller space. This increase in performance has one drawback, though: intense heat is generated during the operation. With a high ratio of surface area to volume and a compact design, the microchannel heat sink (MCHS) becomes a promising means of heat rejection.

The concept of the MCHS was pioneered by Tuckerman and Pease [1], who performed an experimental study on the MCHS and found its immense heat transfer capability. Singh et al. [2] performed an experimental study on a copper microchannel heat sink. They showed that the heat transfer up to 41 MW/m^2 was possible by using their heat sink. A recently researched topic in MCHS is the enhancement of heat-carrying capacity by using passive augmentation techniques. Using two different dimple geometries, Park et al. [3] performed numerical and experimental investigations of a heat sink under laminar flow for passive heat transfer augmentation. Husain and Kim [4] numerically analyzed MCHSs with rib structures with regard to the thermal resistance and pumping power and performed multi-objective shape optimization. Lee et al. [5] numerically evaluated an oblique-fin MCHS for heat transfer enhancement. The oblique-fin MCHS significantly enhanced the heat transfer with little pressure drop penalty. John et al. [6] found that at low Reynolds number (less than 125), the circular-pin fin outperformed others (elliptical and rectangular fins), at medium Reynolds number, the elliptical-pin fin was better, and at high Reynolds number (greater than 200), the square-pin fin showed better performance.

The optimization process facilitates in further exploitation of MCHS; by just a variation of design parameters, a more efficient heat sink can be obtained. Husain and Kim [7] presented optimization of an MCHS with a trapezoidal cross section. They showed that the thermal resistance of the MCHS is considerably reduced by the process of optimization.

The present study is divided into two parts: the first part is dedicated to the optimization of an oblique-fin MCHS, and the second part is a comparative study on performance of various MCHSs. The thermal resistance offered by the MCHS and the pumping power required to drive the fluid through the channels are selected as objective functions for the multi-objective optimization process. For the comparative study, four distinct types of MCHSs (namely, oblique-fin offset, oblique-fin parallel, rectangular-fin offset, and rectangular-fin parallel MCHSs) are selected and their performances are compared with the optimized oblique-fin offset MCHS at various mass flow rates.

II. Microchannel Models and Numerical Methods

Schematic diagrams of the geometries considered in this study are presented in Fig. 1. Figure 1a shows the computational domain with various geometric parameters and boundary conditions. Figure 1b shows the four distinct geometries: viz., oblique-fin offset, oblique-fin parallel, rectangular-fin offset, and rectangular-fin parallel microchannel heat sinks.

Three-dimensional analysis of convective heat transfer through the microchannels was performed numerically using Navier–Stokes equations along with the analysis of heat conduction in the substrate. The flow in the microchannels was assumed to be steady, incompressible, and laminar. The temperature-dependent thermodynamic and hydrodynamic properties of the fluid were accounted for in the solution process [8], but radiation effects were neglected.

To numerically simulate the flow through the microchannel, the governing equations were solved by using a general-purpose computational fluid dynamics code, ANSYS CFX 11.0. The full length of a single periodic channel, shown in Fig. 1a, was selected as the computational domain, to reduce the computation time due to the periodic array of microchannels in the lateral direction. A hexahedral meshing scheme was used for both fluid and solid domains. Deionized ultrafiltered water was selected as the working fluid flowing through

Received 4 April 2010; revision received 10 August 2010; accepted for publication 15 August 2010.

*Professor, Department of Mechanical Engineering, 253 Yonghyun-Dong, Nam-Gu; kykim@inha.ac.kr. Associate Fellow AIAA (Corresponding Author).

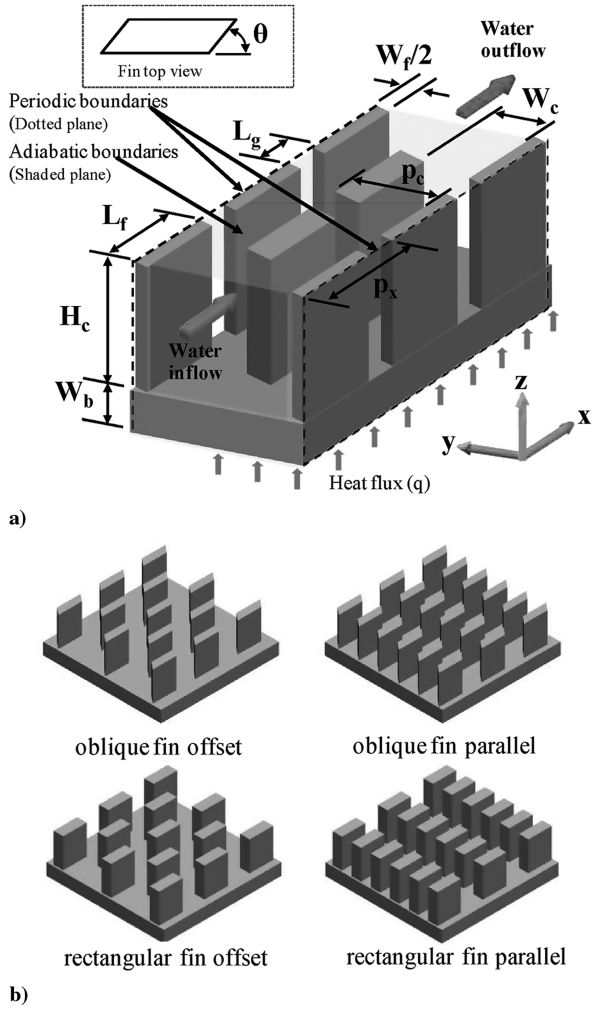

Fig. 1 Schematic diagram of the microchannel heat sinks: a) oblique-fin offset MCHS with the design variables and the boundary conditions and b) various broken-fin MCHSs.

the channels, and the heat sink was considered to be made up of silicon having thermal conductivity of 148 $Wm^{-1}\,K^{-1}$. A no-slip condition was applied at the interior walls of the microchannels. At the inlet of the microchannel, mass flow rate was specified, and at the outlet, zero static pressure (relative) was assigned. Adiabatic boundary conditions were applied at the inlet and outlet portions of silicon. Fluid inlet temperature was taken as 300 K. For the conservative analysis, the top of the microchannel was kept adiabatic and a uniform heat flux was applied at the bottom of the heat sink. The optimization of the oblique-fin offset MCHS was performed at a constant overall mass flow rate. For the comparative analysis, performances of all four different geometries shown in Fig. 1b were evaluated at various mass flow rates.

III. Optimization Techniques

There are many geometric parameters that affect the performance of the MCHS. Among these parameters, four design variables, viz., $p_c/H_c(\alpha)$, $W_f/p_c(\beta)$, $L_f/p_x(\gamma)$, and θ, were formed and selected for the optimization of the oblique-fin offset geometry. The ranges of the design variables are set in view of the past experimental studies on rectangular-fin microchannel heat sinks and presented in Table 1. The numerical analysis is performed for the designs obtained from Latin hypercube sampling (LHS) methods of design of experiment (DOE). The performance of the MCHS is widely analyzed for overall thermal resistance and required pumping power, which are selected as the objective functions to be optimized. The thermal resistance is given by

$$R_{\text{th}} = \frac{\Delta T_{\max}}{qA_s} \tag{1}$$

Pumping power required to drive the fluid through the MCHS is given by

$$P = n \cdot u_{\text{avg}} \cdot A_c \cdot \Delta p \tag{2}$$

The numerical solutions for the objective functions are obtained at the selected design points, and based on these solutions, a continuous approximate response function is obtained by employing the response surface approximation (RSA) [9] model.

In the RSA method, a polynomial function is fitted to the discrete responses obtained by numerical simulations. The polynomial response can be symbolized as

$$y(x) = \beta_0 + \sum_{j=1}^{N} \beta_j x_j + \sum_{j=1}^{N} \beta_{jj} x_j^2 + \sum \sum_{i \neq j}^{N} \beta_{ij} x_i x_j \tag{3}$$

The Pareto-optimal solutions were generated by using the multi-objective evolutionary approach (MOEA), as described by Husain and Kim [7]. The procedure involved in the construction of the Pareto-optimal front consists of several steps [7]: namely, defining design variables and objective functions, obtaining numerical solutions at the DOE selected design sites, constructing an approximate

Table 1 Design variables with their ranges

	Design variables			
	p_c/H_c (α)	W_f/p_c (β)	L_f/p_x (γ)	θ, deg
Lower bound	0.15	0.2	0.4	20
Upper bound	0.30	0.5	0.7	60

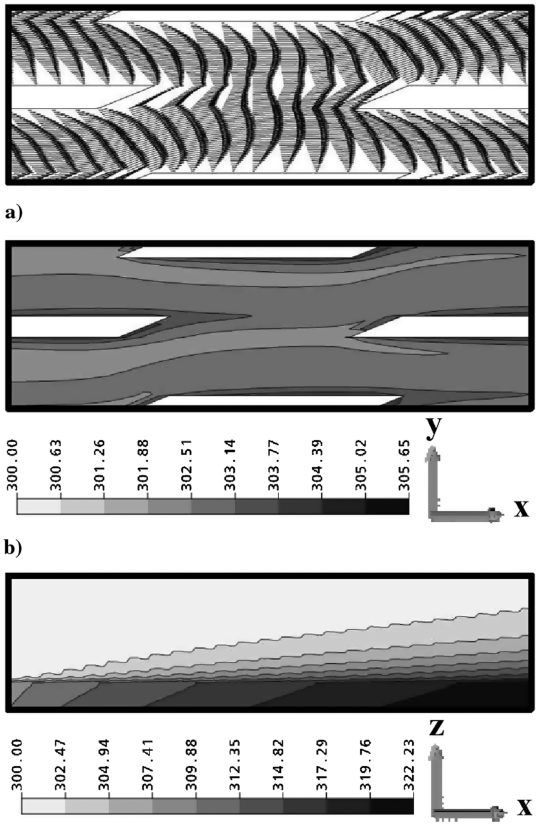

Fig. 2 Velocity and temperature fields: a) velocity vectors on the *x*-*y* plane at $z/L_z = 0.5$, b) temperature contours on the *x*-*y* plane at $z/L_z = 0.5$, and c) temperature contours on the *x*-*z* plane at the center of the channel for $\alpha = 0.171$, $\beta = 0.268$, $\gamma = 0.503$, and $\theta = 22.28°$.

response model for the objective functions, and finding the Pareto-optimal solutions. The global Pareto-optimal solutions were obtained through a hybrid MOEA. In this method, approximate Pareto-optimal solutions are first obtained using the real-coded NSGA-II [10] for the selected objective functions. These solutions are then refined by searching the local optimal solution for each objective function over the whole (NSGA-II-derived) optimal solution using sequential quadratic programming with NSGA-II solutions as initial guesses. *K*-means clustering was performed to select six representative solutions from the Pareto-optimal front.

IV. Results and Discussion

To obtain grid-independent results, test calculations were carried out by varying grid points in all directions. It was observed that the changes in pumping power and thermal resistance were about 5 and 1%, respectively, for a change of grids from 600,000 hexahedral elements to 1,800,000 hexahedral elements, whereas the changes in pumping power and thermal resistance were commonly about 1% for a change of grids from 1,800,000 elements to 2,600,000 elements for the typical grid analysis with the design variables $\alpha = 0.450$, $\beta = 0.333$, $\gamma = 0.500$, and $\theta = 0°$. In view of the above analysis, a grid system with about 2,000,000 hexahedral elements is selected for the numerical computations of the rectangular-fin microchannels. For the channels with oblique fins, twice the number of grid points of the rectangular-fin microchannels are used, due to the doubled computational domain in the lateral direction. The numerical solutions for a smooth microchannel were validated by Husain and Kim [11], who used the same methods of analysis as in this work for a wide range of the Reynolds number.

Breaking continuous fins of conventional smooth MCHS into sectional oblique fins enhances the heat transfer and thus lowers the thermal resistance of MCHS [5]. This enhancement in heat transfer by using oblique fins could be partially attributed to the perturbation of main flow by the injection of crossflow from the oblique channels, as shown in Fig. 2a, and partial increment in heat transfer is due to enhancement of heat transfer area on the oblique surfaces. In smooth MCHSs, convective heat transfer diminishes gradually, due to the formation of a thick thermal boundary layer. In the case of broken-fin MCHSs, however, the thermal boundary layer initializes at the leading edge and collapses at the trailing edge, and thus the formation of the thermal boundary layer is intermittent. This repetitive phenomenon inhibits the thickening of the thermal boundary layer and results in enhancement of heat transfer. Figures 2b and 2c represent the temperature profiles on the *x*-*y* and *x*-*z* planes, respectively. The temperature profile on *x*-*z* plane is scaled down to 0.2 of the full channel length. These profiles exhibit asymmetries due to the crossflow resulting from the oblique channels.

In the RSA method [9], analysis of variance (ANOVA) and regression analysis are implemented to measure the uncertainty in the set of polynomial coefficients of the second-order curve. For thermal resistance the values of R^2, R^2_{adj}, and E_{cv} (based on prediction-error sum-of-squares cross-validation error [9]) are 0.995, 0.992, and 1.37e − 2, respectively, and for pumping power these values are 0.988, 0.979, and 3.8e − 3, respectively.

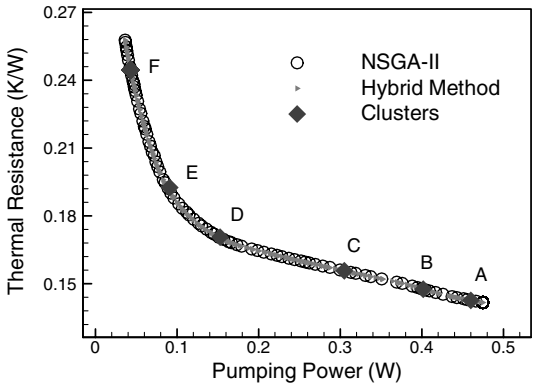

Fig. 3 Pareto-optimal solutions using the NSGA-II, hybrid multi-objective evolutionary approach, and six clusters.

Table 2 Six clusters from the global Pareto-optimal solutions and objective functions.

	Design variables					
Clusters	p_c/H_c (α)	W_f/p_c (β)	L_f/p_x (γ)	θ, deg	P	R_{th}
A	0.150	0.489	0.698	60.00	0.460	0.143
B	0.155	0.466	0.674	60.00	0.402	0.148
C	0.208	0.456	0.700	20.00	0.305	0.156
D	0.300	0.433	0.685	20.00	0.153	0.171
E	0.300	0.324	0.700	20.00	0.091	0.193
F	0.300	0.224	0.700	56.00	0.043	0.245

Approximate, well-distributed, Pareto-optimal solutions with 100 generations and 250 populations were obtained by a real-coded NSGA-II. The crossover and mutation probabilities were set to 0.95 and 0.05, respectively. The crossover and mutation parameters were taken as 15 and 150, respectively. Figure 3 represents the Pareto-optimal front generated by 604 global Pareto-optimal solutions obtained by a hybrid MOEA using RSA as surrogate model. To find the representative solution for a group of nearest solutions, *K*-means clustering was performed. The six representative clusters obtained by *K*-means clustering are shown in Fig. 3. The values of design variables with the corresponding values of objective functions at cluster points are presented in Table 2. The nature of the Pareto-optimal front suggests that the two objective functions are conflicting with each other. Concurrent minimization of both the objective functions is not possible. Each fixed optimal value of one objective can have only one optimal value of the other objective. At the extreme end of the Pareto-optimal front, there exists the lowest value of one

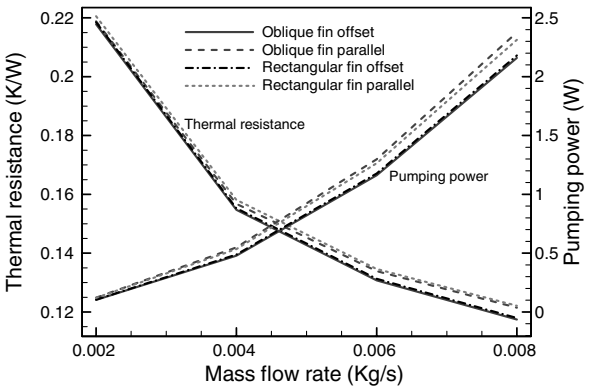

a)

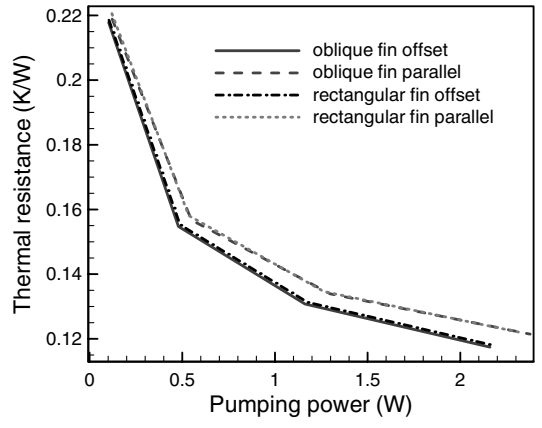

b)

Fig. 4 Variations of thermal resistance and pumping power: a) thermal resistance and pumping power vs mass flow rate and b) thermal resistance vs pumping power.

objective concurrent with the highest value of another objective. No single solution in the collection of all the Pareto-optimal solutions has an edge over the other.

In the second part of this work, a comparative study of four different geometries including the optimized geometry have been performed: namely, oblique-fin offset, oblique-fin parallel, rectangular-fin offset, and rectangular-fin parallel MCHSs. Comparison of conventional smooth MCHS with the oblique-fin MCHS has not been considered here, since it has been already explored that oblique-fin MCHS has lower thermal resistance with insignificant increase in pressure drop than the conventional smooth MCHS [5]. Cluster point B is selected for the design parameters of the other MCHSs under investigation. Objective function values were calculated at various mass flow rates varying from 0.002 to 0.008 kg/s. Figure 4a represents variations of the thermal resistance and the pumping power with mass flow rate. The oblique-fin offset MCHS shows the lowest pumping power as well as the lowest thermal resistance among the considered MCHSs. Variation of thermal resistance with pumping power is shown in Fig. 4b, in which the oblique-fin offset MCHS also has the lowest thermal resistance at the same pumping power. However, the performance of the rectangular-fin offset MCHS is very close to that of the oblique-fin offset MCHS, but there is a large difference between the performances of the offset-fin and the parallel-fin geometries in all the cases shown in Fig. 4. This figure shows that the offset-fin MCHSs perform better than the parallel-fin MCHSs.

V. Conclusions

In the present work, an MCHS with offset oblique fins has been optimized and the performance of this optimum MCHS has been compared with those of four different MCHSs. A multi-objective optimization has been performed with the help of a hybrid evolutionary multi-objective technique. For the optimization, four design variables, viz., the ratios of the pitch of channel to height of channel, width of fin to pitch of channel, length of fin to pitch of fin in the x direction, and the oblique angle, have been selected. The objective functions, viz., thermal resistance and pumping power, have been calculated numerically at the experimental points selected by LHS method. NSGA-II and a local search strategy have been coupled with the RSA model for obtaining Pareto-optimal solutions. It is observed from the Pareto-optimal front that an increase in pumping power tends to decrease in the thermal resistance and vice versa. A comparative study has been carried out among four different MCHSs, including oblique-fin parallel, rectangular-fin offset, rectangular-fin parallel, and optimized oblique-fin offset MCHS. The results show that the two offset-fin MCHSs show similar performances and the offset-fin MCHSs perform better than the parallel-fin MCHSs for thermal resistance and pumping power at the same mass flow rate.

Acknowledgment

This research was supported by the National Research Foundation of Korea (NRF) grant no. 20090083510 funded by the government (Ministry of Education in Science and Technology) through the Multi-Phenomena CFD Engineering Research Center.

References

[1] Tuckerman, D. B., and Pease, R. F. W., "High-Performance Heat Sinking for VLSI," *IEEE Electron Device Letters*, Vol. 2, No. 5, 1981, pp. 126–129. doi:10.1109/EDL.1981.25367

[2] Singh, R., Akbarzadeh, A., Mochizuki, M., Nguyen, T., and Nguyen, T., "Thermal Characterization of a Copper Microchannel Heat Sink for Power Electronics Cooling," *Journal of Thermophysics and Heat Transfer*, Vol. 23, No. 2, April–June 2009, pp. 371–380. doi:10.2514/1.40033

[3] Park, D., Silva, C., Marotta, E., and Fletcher, L., "Study of Laminar Forced Convection Heat Transfer for Dimpled Heat Sink," *Journal of Thermophysics and Heat Transfer*, Vol. 22, No. 2, 2008, pp. 262–270. doi:10.2514/1.33497

[4] Husain, A., and Kim, K.-Y., "Thermal Optimization of a Microchannel Heat Sink with Trapezoidal Cross Section," *Journal of Electronic Packaging*, Vol. 131, No. 2, 2009, Paper 021005. doi:10.1115/1.3103931

[5] Lee, Y-J., Lee, P-S., and Chou, S-K., "Enhanced Micro-Channel Heat Sink Using Oblique Fins," *Proceedings of the ASME 2009 InterPACK Conference*, San Francisco, 2009.

[6] John, T. J., Mathew, B., and Hegab, H., "Characteristic Study on the Optimization of Micro Pin Fin Heat Sink with Staggered Arrangement," 10th AIAA/ASME Joint Thermophysics and Heat Transfer Conference, Chicago, AIAA Paper 2010-4781, 2010.

[7] Husain, A., and Kim, K.-Y., "Microchannel Heat Sink with Designed Roughness: Analysis and Optimization," *Journal of Thermophysics and Heat Transfer*, Vol. 22, No. 3, 2008, pp. 342–351. doi:10.2514/1.34678

[8] Incropera, F. P., and DeWitt, D. P., *Fundamentals of Heat and Mass Transfer*, Wiley, New York, 2002.

[9] Myers, R. H., and Montgomery, D. C., *Response Surface Methodology: Process and Product Optimization using Designed Experiments*, Wiley, New York, 1995.

[10] Deb, K., Agrawal, S., Pratap, A., and Meyarivan, T., "A Fast and Elitist Multi-Objective Genetic Algorithm for Multi-Objective Optimization: NSGA-II," *Proceedings of the Parallel Problem Solving from Nature VI Conference*, Paris, 2000, pp. 849–858.

[11] Husain, A., and Kim, K.-Y., "Shape Optimization of Micro-Channel Heat Sink for Micro-Electronic Cooling," *IEEE Transactions on Components and Packaging Technologies*, Vol. 31, No. 2, 2008, pp. 322–330. doi:10.1109/TCAPT.2008.916791